JGR Atmospheres

RESEARCH ARTICLE
10.1029/2020JD033695

Evaluating Empirical Lightning Parameterizations in Global Atmospheric Models

Douglas C. Stolz[1], Kelsey R. Bilsback[1], Jeffrey R. Pierce[1], and Steven A. Rutledge[1]

[1]Department of Atmospheric Science, Colorado State University, Fort Collins, CO, USA

Key Points:

- Lightning parameterizations are evaluated against monthly Tropical Rain Measuring Mission lightning climatology over the tropics and subtropics
- Lightning parameterization approaches that account for thunderstorm area explain 55%–64% of observed monthly lightning variance
- Using normalized convective available potential energy, warm-cloud depth, cloud condensation nuclei concentration, SHEAR and relative humidity or ice mass fluxes improves on conventional cloud top height approaches for lightning parameterization

Correspondence to:
D. C. Stolz,
doug.stolz@gmail.com

Citation:
Stolz, D. C., Bilsback, K. R., Pierce, J. R., & Rutledge, S. A. (2021). Evaluating empirical lightning parameterizations in global atmospheric models. *Journal of Geophysical Research: Atmospheres*, *126*, e2020JD033695. https://doi.org/10.1029/2020JD033695

Received 12 AUG 2020
Accepted 10 JAN 2021

Author Contributions:
Conceptualization: D. C. Stolz, K. R. Bilsback, S. A. Rutledge
Data curation: D. C. Stolz, K. R. Bilsback
Formal analysis: D. C. Stolz, K. R. Bilsback
Funding acquisition: J. R. Pierce, S. A. Rutledge
Investigation: D. C. Stolz, K. R. Bilsback, J. R. Pierce, S. A. Rutledge
Methodology: D. C. Stolz, K. R. Bilsback, J. R. Pierce
Project Administration: S. A. Rutledge
Software: D. C. Stolz, K. R. Bilsback, J. R. Pierce
Supervision: J. R. Pierce, S. A. Rutledge
Validation: K R. Bilsback

Abstract Lightning fundamentally influences atmospheric chemistry as it is the largest natural source of NO_x in the upper troposphere. To include lightning, global models rely on experimental parameterizations. We use global atmospheric model diagnostics (2.0 × 2.5° horizontal resolution, 38°S–38°N, for the years 2012–2013) to evaluate three lightning parameterizations that are based on: (1) cloud top height, (2) vertical ice-mass flux, and (3) meteorological variables including aerosols. We apply conversions between convective/cloud area and model grid box area in these calculations to compare each parameterization's spatial, temporal, and spectral characteristics with an observed lightning climatology from the Tropical Rainfall Measuring Mission Lightning Imaging Sensor. Domain-wide median values of parameterized lightning differ from observations by a factor of 0.6–3.1. The three parameterizations depict spatial (Pearson correlation (r = 0.80–0.84) and temporal patterns (r = 0.79–0.95) that match observations well. The parameterized median land-ocean lightning contrast ranges from a factor of 2.82 (using environmental factors with aerosols) to 596.0 (using cloud top height), compared to 22.9 in observations. One-to-one comparisons suggest that lightning parameterizations can explain approximately 55%–64% of the observed monthly lightning variance, depending on the parameterization. The highest correlation and minimum error bias statistics (e.g., Logarithmic Mean Bias, LMB) are found for the lightning parameterization that employs environmental factors with aerosols (r = 0.80, LMB = +0.002), whereas comparable correlation and generally higher error bias are found using vertical ice fluxes (r = 0.80, LMB = +0.27) and cloud top height (r = 0.74, LMB = −0.08). We show how the biases in lightning estimates are sensitive to uncertainties in the convective area and suggest ways to minimize bias overall.

Plain Language Summary This study investigates how lightning can be more accurately represented in global atmospheric models, using three different approaches: (1) based on environmental characteristics (potential energy, warm cloud depth, humidity, wind shear and atmospheric aerosols); (2) based on the vertical transport of ice particles; or (3) based on the peak thunderstorm height. A novel aspect of this research is that implementations of monthly lightning estimates incorporate the approximate areal extent of thunderstorms (convective area)/number of thunderstorms within model grid boxes. We document the performance of each lightning approximation method and its respective predictions for the frequency of occurrence for various lightning intensities over land and ocean using a single atmospheric model for simplicity. The results suggest that these lightning estimation approaches account for about 55%–64% of the monthly variations in a test sample of satellite lightning observations (without artificial scaling). Recent approaches to model lightning occurrence (e.g., approaches [1] and [2] above) show modest improvements in accuracy and reduced error bias compared to the conventional cloud top height approach (i.e., approach [3] above). We discuss ways to further improve monthly lightning estimates in global atmospheric models as well as the relationship between lightning and atmospheric chemistry under future climate change scenarios.

1. Introduction

Lightning is the largest natural source of NO_x in the upper troposphere across the tropics and subtropics (Schumann & Huntrieser, 2007) and NO_x species are chemical precursors to ozone, which is a veritable greenhouse gas and air pollutant. Yet, accounting for lightning-generated NO_x in numerical models (e.g., Finney et al., 2016; Grewe et al., 2001; Price et al., 1997) remains challenging because the microphysical mechanisms which are believed to generate cloud electrification (e.g., Latham et al., 2007; MacGorman & Rust, 1998; Takahashi, 1978) involve physical time and space scales that are much finer than the resolution

Writing – original draft: D. C. Stolz
Writing – review & editing: K. R. Bilsback, J. R. Pierce, S. A. Rutledge

of standard global atmospheric models. This mismatch in spatio-temporal scale can lead to appreciable errors in predicted versus observed lightning distributions (Tost et al., 2007). Therefore, to adequately characterize the global evolution of atmospheric chemistry, more accurate lightning representations need to be implemented in global models.

A conventional approach to address the aforementioned problem of estimating lightning in global models is to use a lightning parameterization, a technique that implicitly represents lightning based on theoretical or empirical relationships among lightning, convective clouds, and/or aspects of the surrounding atmospheric environment (see Lopez, 2016; Clark et al., 2017, and references therein) that can be represented in global models. One of the most widely used schemes to parameterize global lightning behavior is based on an exponent-power relationship relating cloud top height to lightning (Price & Rind, 1992, 1993, 1994), with modifications that account for intra-cloud and cloud-to-ground lightning (i.e., total lightning). Price and Rind (1992, "PR92" hereafter) aggregated lightning characteristics from three sets of continental field measurements over four years to derive an empirical lightning flash rate parameterization with units of (fl. min^{-1}) per storm using cloud top height (km). When they implemented their approach (derived from continental thunderstorms over the United States) over larger domains, they documented significant overestimates of lightning flash rate compared to observations, most notably over oceans. PR92 modified the parameterization based on hypothesized differences in updraft velocity over continents and oceans and the subsequent result was shown to be more consistent with observations. Price and Rind (1994) developed a spatial correction factor (see discussion in Allen & Pickering, 2002) that is commonly used to quantify how the average cloud top height diminishes when averaging cloud characteristics over progressively larger grid box areas. However, this factor does not account for the number of thunderstorms per grid box; we argue that the conversion of lightning flash rate per storm to flash density (fl. min^{-1} km^{-2} $_{grix\_box}$) in a model grid box needs to account not only for the changes in the average cloud type height, but also for the number of thunderstorms in the model grid box.

Following previously documented correspondence between lightning and ice-hydrometeor concentrations, ice-water path (e.g., Barthe et al., 2010; Liu et al., 2012; McCaul et al., 2009; Petersen et al., 2005; Petersen & Rutledge, 2001), and vertical motion, Finney et al. (2014; referred to as "F14" hereafter) developed total lightning parameterizations based on the vertical ice-mass flux for both continental and oceanic regions. These experimental relationships used one year of Tropical Rain Measuring Mission (TRMM) Lightning Imaging Sensor (LIS) observations and reanalysis meteorological products for training. For model grid-box lightning estimates, F14's fit to lightning observations over continents was found to be better than over oceans (Pearson correlation, $r = 0.63$ over continents vs. $r = 0.25$ over oceans). The output from their approach is flash density (with units of [fl. s^{-1} $m^{-2}$$_{grix_box}$]). To derive this metric, F14 used model grid-box area as the area normalization factor and made adjustments for both convective mass flux and cloud fraction in each model grid box. With the same underlying reanalysis, F14's parameterization slightly outperformed estimates of flash density derived using PR92's cloud top height approach. Note, in their comparison, F14 applied the conversion factor from Price and Rind (1994) to the PR92 formulations for continents and oceans, yet they did not account for the number of storms per grid box. Instead, they opted to use a dimensionless scaling factor of 0.05 to artificially match PR92 with LIS observations.

Stolz et al. (2017a, referred to as "S17" hereafter) used global reanalysis (at a horizontal resolution of approximately 2.0° latitude × 2.5° longitude) to specify the approximate environmental characteristics (normalized convective available potential energy, NCAPE; cloud condensation nuclei concentration, CCN; warm-cloud depth, WCD; relative humidity, RH; and vertical wind shear, SHEAR) surrounding more than 260,000 individual convective features (e.g., Liu et al., 2008; Stolz et al., 2015) with total lightning observed in the Tropical Rainfall Measuring Mission satellite climatology over eight successive years, 2004–2011. S17 then used multiple-linear regression to develop total lightning parameterizations based on the aforementioned environmental factors over continents and oceans separately within the TRMM domain (38°S–38°N, across all longitudes). S17 incorporated CCN as a predictor, based on the findings of earlier studies (Michalon et al., 1999; Stolz et al., 2015, 2017b and references therein), which suggested CCN concentrations explained a non-negligible fraction of lightning variance, apart from background meteorology. The output from S17's lightning parameterization is in terms of total flash density (with units of [fl. min^{-1} $km^{-2}$$_{conv_area}$]), which uses the convective precipitation area discerned by the TRMM precipitation radar for the area normalization.

Stolz et al. (2015) suggested that reporting lightning flash rate per convective feature (i.e., without explicitly normalizing for convective area) can be misleading because high flash rates can result from integrating low flash density over large precipitation features. Furthermore, using satellites to observe convective features complicates lightning flash rate estimation per storm object because the edge of a convective feature could extend beyond the boundaries of the satellite's field of view. Explicitly normalizing lightning flash rate by area mitigates the problem of incompletely observing a given thunderstorm feature and more closely describes the average lightning intensity at the feature level. S17's approach has yet to be adapted for use in a global model and also has yet to be compared to other lightning parameterizations or a temporally independent set of lightning observations in the tropics and subtropics.

There are many additional global lightning parameterizations that have been proposed in the literature (e.g., Allen & Pickering, 2002; Clark et al., 2017; Lopez, 2016), however we have chosen to highlight and examine a subset of approaches: PR92, F14, and S17. The chosen approaches account for total lightning (instead of only cloud-to-ground lightning) over continents and oceans. Even though PR92 was derived using thunderstorm data over various regions of the United States, the authors later adapted their approach to address land-ocean differences, and we include PR92 in the current study because the parameterization has been tested in global models for more than 25 years. F14 was derived to estimate total lightning produced by the subset of cloudy areas in a model grid box and more closely incorporates the ice-hydrometeor fluxes that are theorized to be central to cloud electrification. Like PR92, the S17 approach represents lightning produced by individual convective areas, except S17 explicitly normalizes for convective area and can readily be converted to model grid-box lightning estimates (similar to F14), if the convective fraction is provided.

The objectives of this study are to rectify inconsistencies in the nominal units of the approaches by PR92, F14, and S17 using the same global model for comparison as well as to evaluate these lightning parameterizations against observed total lightning climatology. We investigated whether lightning estimates based on diagnosed cloud/environmental characteristics (i.e., defined using model output) could provide both precise and accurate estimates of total lightning over continents and oceans. Without any artificial scaling coefficients, we examined how well the chosen lightning parameterizations (that were derived based on thunderstorm/convective cloud/convective feature areas) compared to an independent set of monthly lightning observations over multiple years when differences in basic lightning quantities (i.e., lightning flash rate vs. flash density) and area normalization units are accounted for during implementation.

2. Data and Methods

In these investigations, we used meteorological quantities from reanalysis and output from chemical-transport model simulations to compute monthly lightning estimates based on three separate lightning parameterizations detailed in the literature. The chosen geographic area for evaluation spans the Tropical Rainfall Measuring Mission (Kummerow et al., 1998) satellite's domain (38°S–38°N) and the horizontal resolution for this analysis is 2.0° latitude × 2.5° longitude. To ensure the highest lightning observation data quality, we truncated our evaluation period to the time from January 2012 to December 2013 (e.g., following Albrecht et al., 2016). We opted not to study the time period from 1998 to 2003 (outside of S17's training period from 2004 to 2011 and partially overlapping with F14's training period from 2002 to 2011) due to inconsistency in the observational lightning record, and changes to the TRMM's viewing geometry (the TRMM satellite underwent a boost maneuver in 2001, which increased the field of view). The approach is to convert parameterized lightning estimates for PR92 and S17, which are initially representative of thunderstorm/convective feature area, to model grid-box-equivalent flash density values. F14's approach, which is summarized in Finney et al. (2018), uses model output for cloud area diagnostics directly and therefore avoids the need to make the convective area conversion. The investigation will compare average monthly values of output from PR92, F14, and S17 to observed lightning values over continents and oceans to describe spatial, temporal, and spectral aspects of variability.

2.1. Lightning Data

During 17+ years in orbit, the TRMM satellite documented the spatial and temporal lightning frequency signatures of hundreds of thousands of precipitation areas in the tropics/subtropics using the K_u-band

precipitation radar (PR) and the LIS instrument onboard. The data that specifically characterize the observational lightning component for this study come from the gridded TRMM total lightning climatology (Cecil, 2006; Cecil et al., 2014; available, http://dx.doi.org/10.5067/LIS/LIS-OTD/DATA309). The TRMM satellite completed 16 orbits per day resulting in approximately 2–4 overpasses over a given location each day. Each orbit consisted of "snapshots" lasting about 90–100 s in duration. The LIS instrument detected total lightning events by measuring radiant emissions in the 777.4 nm optical band from both cloud-to-ground and intra-cloud lightning. Cecil et al. (2014) binned lightning flashes geographically at 2.5 × 2.5° horizontal resolution and the number of detected flashes was scaled by the LIS instrument's detection efficiency (Boccippio et al., 2002; Christian et al., 1992).

To create monthly lightning time series from daily gridded LIS lightning data, Cecil et al. (2014) first used a 99-day boxcar moving average followed by a low-pass filter (98-day window length), which roughly accounts for observing convective activity over a given location at each hour of the day (local time) at least twice (D. Cecil, pers. communication). Cecil et al. (2014) then used a 7.5°-wide boxcar average to smooth the data in each spatial dimension. Cecil et al. (2014) named the resulting TRMM-based lightning product the "Low-Resolution Monthly Time Series" (LRMTS; https://ghrc.nsstc.nasa.gov/hydro/details/lolrmts), and the LRMTS represents the monthly average flash density by extracting the data point at the middle of each month (roughly the 15th day). Following from above, we use a temporal subset of the LRMTS as the climatological observation set for the current study.

2.2. Environmental Variables Used in Lightning Parameterizations

Environmental inputs were calculated from instantaneous and 3 h averaged MERRA-2 meteorological variables, using Python's MetPy package (https://unidata.github.io/MetPy/latest/index.html). The MERRA-2 data have an underlying 0.5 × 0.625° horizontal resolution (Bosilovich et al., 2015; Gelaro et al., 2017), but the reanalysis data (e.g., temperature, relative humidity/moisture, and horizontal wind components) were coarsened to 2.0 × 2.5° horizontal resolution to match the aerosol component input for estimating lightning via the parameterizations by S17. We refer the reader to a discussion in Gelaro et al. (2017) concerning the inputs to MERRA-2's data assimilation routine as well as errors/biases in the reanalysis.

The average relative humidity (RH) (%) from MERRA-2 was calculated by taking the arithmetic mean value between model layers $\eta = 0.85$–0.5 (i.e., ~850–500 hPa). Environmental wind shear (SHEAR) was formulated according to the norm of eastward (u) and northward (v) wind components (m s^{-1}), that is, $\mathrm{sqrt}[(u_1 - u_2)^2 + (v_1 - v_2)^2]$, between $\eta = 1.0$ and $\eta = 0.5$ (e.g., ~surface-500 hPa level). We used vertical profiles of pressure, temperature, and RH as inputs from MERRA-2 to estimate the WCD; we calculated the lifted condensation level (i.e., cloud base height) using the surface temperature and dew-point temperature, and subsequently estimated WCD as the vertical distance between cloud base and the local freezing level in the column (m). Convective available potential energy (CAPE) was calculated by a pseudoadiabatic approximation via lifting a surface-based parcel, using vertical profiles of pressure, temperature, and dew-point temperature from MERRA-2. We took the quotient of CAPE (J kg^{-1}) and the depth of theoretical surface-based parcel's positive buoyancy to derive normalized CAPE, or NCAPE (J kg^{-1} m^{-1}). Note, no lightning computations were performed in grid boxes where NCAPE and convective area were zero. Furthermore, Stolz et al. (2015) developed their approach by filtering out convective features with WCD < 2,000 m or WCD > 5,000 m, based on the relative frequency of convective features with ascribed WCD above or below those thresholds in the TRMM domain sample. We adopted a similar convention here when running calculations for S17.

Convective fraction, conv_frac ($m^2_{\mathrm{conv\_area}}$ $m^{-2}_{\mathrm{grid\_box}}$), was calculated at the $\eta \sim 0.44$ (pressure ~440 hPa) level using the following formula:

$$\mathrm{conv\_frac} = \Phi_{\mathrm{mass},m} \,/\, \left(\rho \cdot w_{\mathrm{globe}}\right) \tag{1}$$

where $\Phi_{mass,m}$ is the upward moist convective mass flux (kg m^{-2} s^{-1}) from MERRA-2, density, ρ (kg m^{-3}) was calculated using the ideal gas law with reanalysis pressure and temperature, and the assumed vertical velocity, w_{globe}, was set to a constant 0.5 m s^{-1}. The assumption for $w_{\mathrm{globe}} = 0.5$ m s^{-1} is based on earlier observational studies of tropical cumulonimbus clouds within the TRMM domain; using data collected during

aircraft penetrations of tropical cumulonimbus clouds, LeMone and Zipser (1980) documented sustained upward vertical velocity of at least 0.5 m s^{-1} for 50% of in-cloud flight legs extending 500 m in length or longer (at altitudes of 4,300–8,100 m).

The assumption of vertical velocity has significant impacts on the lightning predictions, so we performed a rigorous sensitivity analysis on the vertical velocity parameter. Based on Equation 1, we estimated a resultant convective area via multiplying the nominal model grid box area by the convective fraction. If the convective area was zero, then no lightning computations were performed. We acknowledge that the constant global vertical velocity specified here is a crude assumption to estimate for convective fraction, yet we use it as a control value by applying it to both the PR92 and S17 parameterizations for analysis (see the vertical velocity sensitivity analysis in Section 3.4 below). Note that cloud fraction (as opposed to convective fraction) is a MERRA-2 model diagnostic, and it will be used in the implementation of the F14 lightning parameterization (described below in Section 2.4.2).

2.3. Chemical Transport Model Output

To estimate aerosol concentrations in the atmosphere within the TRMM domain, we used the GEOS-Chem model (v12.0.3; http://doi.org/10.5281/zenodo.1464210) with MERRA-2 offline meteorological fields (https://gmao.gsfc.nasa.gov/; Gelaro et al., 2017). We ran the Tropchem model configuration with the TwO Moment Aerosol Sectional (TOMAS) online aerosol microphysics scheme (Adams & Seinfeld, 2002; Trivitayanurak et al., 2008) for two model years: 2012 and 2013 (plus 1 month of model spin up time for each year). Tropchem includes the full GEOS-Chem mechanism in the troposphere (~280 species and ~645 reactions). The TOMAS online microphysics scheme was run with 15 size bins (3 nm–10 μm) and included nucleation, condensation, and coagulation microphysics processes as well as size-resolved emissions, dry and wet deposition, and aqueous sulfur chemistry (Kodros & Pierce, 2017; Pierce & Adams, 2009; Pierce et al., 2013). Size-resolved aerosol tracers included sulfate, sea salt, organic aerosols, black carbon, and mineral dust. For anthropogenic emissions, we used the Emissions Database for Global Atmospheric Research (EDGARv4.3; Crippa et al., 2016) as the base inventory with regional overwrites (MIXv2010, DICE-Africa, NEI2011, APEI, BRAVO, and EMEP) (Crippa et al., 2016; Kuhns et al., 2005; Li et al., 2017; Marais & Wiedinmyer, 2016). For natural emissions, we used the GFED4 for biomass burning, MEGAN for biogenic emissions, the Jaeglé scheme for sea salt emissions, and the DEAD scheme for natural dust (Guenther et al., 2012; Jaeglé et al., 2011; Randerson et al., 2017; Zender et al., 2004). Secondary organic aerosol followed a simple scheme by Pai et al. (2019).

For the current study, estimates of CCN [cm^{-3}] from GEOS-Chem-TOMAS simulations were calculated as the mean number of particles with diameters greater than 40 nm (N40) between model levels $\eta = 1.0$–0.85 (i.e., pressure ~1,000–850 hPa, where corresponding pressure levels are calculated by multiplying surface pressure by model level, η). D'Andrea et al. (2013) presented annual-mean statistics comparing GEOS-Chem estimates and ground-based aerosol observations. Their findings suggest that estimates of N40 from GEOS-Chem are routinely within a factor of two compared to observations. The CCN proxy was calculated as a three-hour average based on GEOS-Chem model output at 2.0 × 2.5° horizontal resolution, corresponding to the discrete output times of MERRA-2 offline meteorological data (see Section 2.2 above).

2.4. Implementing lightning Parameterizations

We used separate parameterizations for continental and oceanic regions as in the original studies (e.g., PR92, F14, and S17). Continental and oceanic grid box delineations followed from the conventions in the underlying GEOS-Chem modeling system, which use fractional land/ocean area from the model grid metadata. Land is designated for areas where the fraction of land is nonzero, while ocean is designated where the fraction of ocean is greater than 0.5. Since these criteria are not mutually exclusive, the latter ocean-fraction criterion was adopted where there were overlapping designations. For example, grid boxes that theoretically contain small islands covering only a small portion of a grid box (e.g., <5%) were labeled as ocean areas. Since many global models coarsely represent underlying topography, we believe this is a valid assumption to distinguish land and oceanic areas in global atmospheric modeling context. These land-sea mask values were referenced throughout our analysis to differentiate lightning characteristics and compile relevant statistics.

The PR92, F14, and S17 lightning parameterizations are derived from experimental characterizations of lightning observed in association with deep convective clouds. However, without incorporating nested convection-allowing model sub-routines, global atmospheric models do not explicitly resolve individual convective elements. Thus, a method is needed to translate parameterized flash density estimates into measures that are representative of the average conditions within a relatively coarse-resolution model grid box (e.g., using Equation 1). In this study, we pay specific attention the native units of each parameterization to ensure the formulations are ultimately consistent before comparing monthly lightning estimates in model grid boxes.

2.4.1. Lightning parameterization Using Cloud Top Height (PR92)

PR92 developed empirical relations for lightning flash rate per thunderstorm based on cloud top height (km) (inferred using radar) for continental cloud populations. The authors adapted a relationship applicable over maritime regions thereafter. Here, we estimated cloud top height using the upward moist convective mass flux (3 h averaged) reanalysis product from MERRA-2. Using, the MetPy "thickness_hydrostatic ()" function, the cloud top height was estimated by calculating the vertical distance between the surface and the midpoint of the highest model layer in the column with non-zero convective mass flux (a description of the vertical grid resolution used for these simulations is available at, http://wiki.seas.harvard.edu/geos-chem/index.php/GEOS-Chem_vertical_grids#47-layer_reduced_vertical_grid). Following from observations detailed in Williams (1985) that were used to develop the PR92 approach, we interpret the native units of the total lightning flash rate for PR92 as "per thunderstorm" (fl. $min^{-1}{}_{storm}$) over land and oceans. The empirical formulations based on cloud top height follow below:

$$F_{l,\mathrm{PR92}} = \mathrm{C} \cdot 3.44 \cdot 10^{-5} \cdot \mathrm{H}^{4.9} \text{ for land} \tag{2a}$$

$$F_{\mathrm{o,PR92}} = \mathrm{C} \cdot 6.4 \cdot 10^{-4} \cdot \mathrm{H}^{1.73} \text{ for ocean} \tag{2b}$$

where H is cloud top (km) and C is the dimensionless intensity correction factor that accounts for reductions in H that result from averaging convective-cloud-related diagnostics within relatively coarse model grid boxes (see Figure 1 in Price & Rind, 1994).

Bang and studied lightning-producing precipitation features observed by the TRMM satellite over continental and tropical oceanic regions and found that the median size of thunderstorm complexes ($km^2{}_{storm}$) was approximately 12,300 km^2 over ocean versus 900 km^2 over continental areas. We estimated the convective area in each of our grid boxes by multiplying the model grid box area by the convective fraction (i.e., Equation 1). We then estimated the number of thunderstorm complexes in a model grid box by taking the quotient of the convective area and an assumed thunderstorm complex area (1,000 km^2 over land and 10,000 km^2 over ocean). Next, we estimated the total lightning flash rate in the model grid box for PR92 by the product of Equation 2 and the resulting approximate number of thunderstorm complexes. Finally, the flash density (fl. $min^{-1}\ km^{-2}{}_{grid\_box}$) was found via normalizing the total lightning flash rate by the nominal grid box area.

2.4.2. Lightning parameterization Using Vertical ice Mass Flux (F14)

F14 compared flash density observations from the same LRMTS climatology by Cecil et al. (2014) that we employ in the current study to ice-hydrometeor quantities from reanalysis. F14 derived a parameterization that depends on the vertical ice mass flux, φ_{ice}, ($kg_{ice}\ m_{grid\_box}{}^{-2}\ s^{-1}$) in the mid-troposphere (i.e., at $\eta \sim 0.44$ or pressure ~440 hPa):

$$\varphi_{\mathrm{ice}} = \left(q_{\mathrm{ice}} \cdot \Phi_{\mathrm{mass},m}\right) / \text{ cloud\_fraction} \tag{3}$$

where q_{ice} [$kg_{ice}\ kg_{air}{}^{-1}$] is the mass fraction of (nonprecipitating) cloud-ice water from MERRA-2 (pressure = ~440 hPa, $\eta = 0.440$, 3 h averaged) and $\Phi_{mass,m}$ ($kg_{air}\ m^{-2}{}_{grid\_box}\ s^{-1}$) is the grid-box average upward moist convective mass flux from MERRA-2 (Pressure = ~440 hPa, $\eta = 0.44$, 3 h averaged). The cloud_fraction in Equation 3 is specified directly using the cloud fraction diagnostic from the MERRA-2 data ($m^2{}_{cloud\_area}\ m^{-2}{}_{grid\_box}$) (see supplemental methodology of Finney et al., 2018). Using the vertical ice mass flux, flash density (fl. $s^{-1}\ m^{-2}{}_{grid\_box}$) for the F14 parameterization is as follows:

$$F_{l,F14} = 6.58{\cdot}10^{-7}{\cdot}\varphi_{ice} \text{ for continents} \tag{4a}$$

$$F_{o,F14} = 9.08{\cdot}10^{-8}{\cdot}\varphi_{ice} \text{ for ocean} \tag{4b}$$

The leading constants in Equation 4 are based on F14's least squares linear regression results comparing flash density observations (i.e., from LRMTS) with vertical ice mass flux from reanalysis. Note, in their derivation of convective area, F14 multiplied the grid-box average vertical mass flux by the convective fraction. As a slight variation in this study, Equation 4 represents average flash density in the grid box accounting for convective updraft area using the moist convective vertical mass flux variable (from MERRA-2).

2.4.3. Lightning parameterization Using Environmental Factors (S17)

The parameterization by S17 provides estimates of flash density for individual convective features with attributed environmental parameters. S17 used logarithmic transforms to fit flash density (fl. min^{-1} $km\text{-}_{conv\_area}{}^{-2}$) to physically related environmental variables:

$$\begin{aligned}\log_{10}\left(F_{l,S17}\right) = {} & 1.037 + 0.171 * \log_{10}\left(\text{NCAPE}\right) + 0.169 * \log_{10}\left(\text{CCN}\right) - 0.723 * \ldots \\ & \log_{10}\left(\text{WCD}\right) + 0.084 * \log_{10}\left(\text{SHEAR}\right) - 0.623 * \log_{10}\left(\text{RH}\right)\end{aligned} \tag{5a}$$

$$\begin{aligned}\log_{10}\left(F_{o,S17}\right) = {} & 3.413 + 0.300 * \log_{10}\left(\text{NCAPE}\right) + 0.174 * \log_{10}\left(\text{CCN}\right) - 1.521 * \ldots \\ & \log_{10}\left(\text{WCD}\right) + 0.011 * \log_{10}\left(\text{SHEAR}\right) - 0.352 * \log_{10}\left(\text{RH}\right)\end{aligned} \tag{5b}$$

where F_l and F_o denote flash density for land and ocean, respectively. The units are (J kg^{-1} m^{-1}) for NCAPE, (cm^{-3}) for CCN, (m) for WCD, (m s^{-1}) for SHEAR, and (%) for RH (see Sections 2.2 and 2.3 for complete descriptions of these variables). As a modification to S17's original approach, we compute lightning estimates using instantaneous environmental quantities within individual model grid boxes to emulate implementing the parameterization in a global atmospheric model framework as opposed to computing "inflow parcels" using the European Center for Medium-range Weather Forecasts Interim Reanalysis (e.g., Stolz et al., 2015). We use the same convective area quantity as described above (i.e., Section 2.4.1) to find the aggregate total lightning in a model grid box; after calculating linear lightning estimates from logarithmic output of Equation 5, we then normalized by the nominal grid box area to get flash density with units (fl. min^{-1} $km^{-2}{}_{grid\_box}$).

2.4.4. Preparing Observed and Parameterized Lightning for Comparison

Prior to doing observation-model comparisons, we re-gridded observational data from the Cecil et al. (2014) climatology and MERRA-2 to match at the model resolution of 2.0° latitude × 2.5° longitude. To approximate the spatial and temporal smoothing of the observation data set in parameterizations, we smoothed the parameterized lightning estimates with 6.0° latitude × 7.5° longitude spatial and 99-day boxcar temporal averages, following the methodology of Cecil et al. (2014). Next, we averaged the geospatial grids of smoothed three-hourly parameterized lightning values along their temporal dimension for each month between 2012 and 2013 to obtain monthly average values. As final pre-processing step, we applied appropriate temporal conversions (i.e., 60 min h^{-1}, 24 h d^{-1}, and 365 days yr^{-1}) to arrive at common units for flash density (fl. yr^{-1} $km^{-2}{}_{grid\_box}$), which are used elsewhere in the literature.

3. Results

3.1. Geographic and Temporal Distributions

Figure 1 shows the time-averaged spatial distributions of monthly flash density from observations and the three parameterizations (PR92, F14, and S17) during the evaluation period (2012–2013). Logarithmic scaling immediately draws out the land-ocean contrast–differing at least by a factor of 10 (e.g., Christian et al., 2003), on average, in this two-year subset of the observed TRMM climatology (Figure 1a). Observed

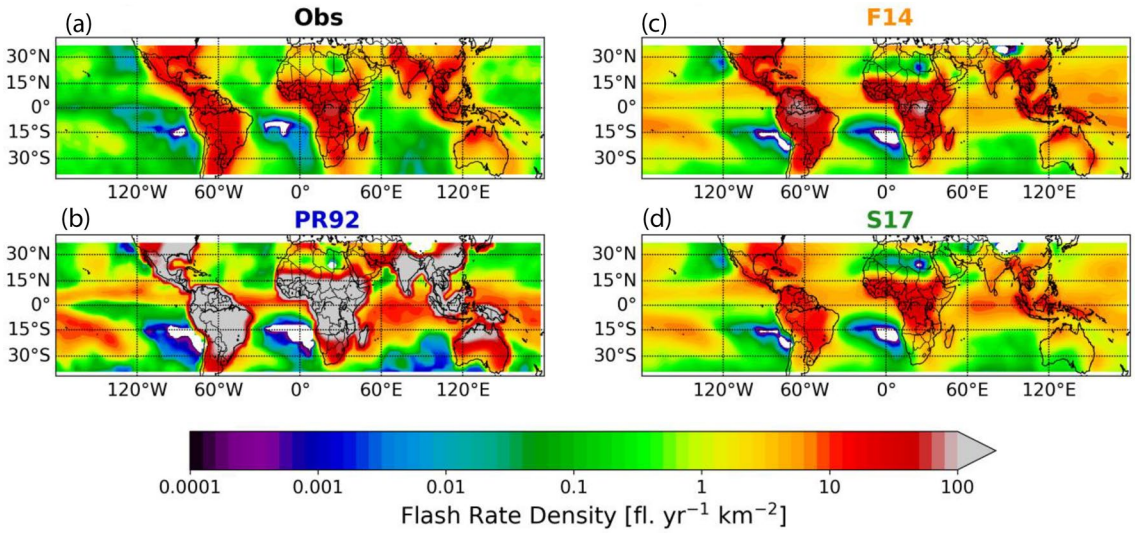

Figure 1. Temporal average of total lightning flash density (fl. yr^{-1} km^{-2} $_{\text{grid\_box}}$) for the evaluation period (all months between January 1, 2012 and December 31, 2013) observed by (a) TRMM LIS (Low-Resolution Monthly Time Series, LRMTS) and modeled using lightning parameterizations by (b) PR92, (c) F14, and (d) S17. See the text in Section 2 for a technical definition of lightning parameterizations. TRIM, tropical rain measuring mission; LIS, lightning imaging sensor.

monthly average lightning values are generally greater than 10 fl. yr^{-1} km^{-2}$_{\text{grid\_box}}$ over continents and less than 1.0 fl. yr^{-1} km^{-2}$_{grid_box}$ over remote ocean, whereas extreme values (i.e., from the 5th to 95th percentiles) span more than four orders of magnitude across land and ocean. In coastal regions where the prevailing low-level wind is offshore (e.g., over the Gulf Stream and Kuroshio currents, west of Central America and sub-Saharan Africa, as well as downstream of South America, South Africa, and Australia) greater flash density persists much farther offshore; these are commonly observed offshore lightning maxima. Not counting monthly lightning values of 0.0 fl. yr^{-1} km^{-2}$_{\text{grid\_box}}$, the observed domain-wide median monthly flash density is 0.60 fl. yr^{-1} km^{-2}$_{\text{grid_box}}$, and the observed land-ocean contrast (taken as the ratio of the median of flash rate density over land vs. ocean, during all months of the evaluation period) is 22.9. A summary of monthly lightning statistics for observations and the parameterizations (to be referenced below) is provided in Table 1.

The geographic distributions of parameterized flash density (without any global or localized dimensionless scaling factors, as was used by Tost et al., 2007; Murray et al., 2012; Lopez, 2016, for example) are shown in Figures 1b–d. Without including lightning values of 0.0 fl. yr^{-1} km^{-2}$_{\text{grid\_box}}$, the domain-wide median lighting flash rate density (without averaging across all months of the evaluation period) values are 0.361, 1.88, and 1.39 fl. yr^{-1} km^{-2}$_{\text{grid_box}}$ for PR92 (Figure 1b), F14 (Figure 1c), and S17 (Figure 1d), respectively (see Table 1 for domain-wide, land-only, and ocean-only quantiles). Therefore, the parameterized lightning outputs from PR92 underestimate domain-wide observations by approximately 40% while F14 and S17 overestimate observations by approximately 212% and 131%, respectively, based on domain-wide median values. As shown in Table 1, the land-ocean contrast for each lightning parameterization is approximately 596.0 for PR92, 6.02 for F14, and 2.81 for S17. Aspects of the general circulation are captured to varying degrees by the different lightning parameterizations, such as local maxima downstream of major continents. F14 and S17 provide smoother transitions in coastal regions, while the coastal transitions resemble a step-change using PR92. The spatial linear correlation between the mean observed and parameterized lightning distributions is $r = 0.83$ for F14, $r = 0.80$ for PR92, and $r = 0.84$ for S17.

Spatial distributions of average errors (i.e., averaged in the temporal dimension) in flash density are shown in Figure 2 for each of the parameterizations in turn. The red shading indicates areas where the parameterization overestimates observations, whereas blue shading indicates areas where the parameterization underestimates observations, on average. A Wilcoxon signed-rank test, which accounts for serial correlation in paired data samples (see Wilks, 2011), was used to quantify the statistical significance of these "local," grid-box comparisons. The null hypothesis, H_0, states that the medians of the distributions of

Table 1
Total lightning flash density (fl. yr^{-1} km^{-2} $_{grid\_box}$) statistics for January 1, 2012–December 31, 2013 (38°S–38°N, across all longitudes) based on observations from the Lightning Imaging Sensor low-resolution monthly time series and the lightning flash density parameterizations by PR92, F14, and S17

Lightning data	Region	5th	25th	Median	75th	95th
LIS LRMTS	Full domain	2.70×10^{-3}	0.110	0.603	3.79	22.8
	Land only	0.131	1.95	7.28	17.8	40.5
	Ocean only	1.27×10^{-3}	0.06	0.318	1.21	8.59
PR92	Full domain	5.56×10^{-4}	2.30×10^{-2}	0.361	18.1	400.0
	Land only	9.21×10^{-2}	5.54	70.3	314.0	664.0
	Ocean only	3.14×10^{-4}	1.06×10^{-2}	0.118	0.717	89.7
F14	Full domain	1.86×10^{-4}	0.293	1.88	6.00	36.7
	Land only	1.94×10^{-3}	1.08	8.13	28.3	65.6
	Ocean only	7.43×10^{-5}	0.212	1.35	4.15	10.1
S17	Full domain	5.65×10^{-5}	0.196	1.39	4.77	14.9
	Land only	1.16×10^{-6}	0.251	3.29	10.9	26.6
	Ocean only	1.07×10^{-4}	0.185	1.17	3.64	9.31

The three entries in each table cell represent domain-wide (top), land-only (middle), and ocean-only (bottom).

paired samples (i.e., parameterized and observed monthly lightning data) are the same, whereas the alternative hypothesis, H_a, holds that the two samples were drawn from different underlying distributions. We evaluated H_0 using two-tailed probabilities with a 5% significance level threshold. Using the PR92 (Figure 2a) parameterization results in average flash density errors over land masses and many tropical oceanic areas of at least 100% relative to observations, and the PR92 parameterization underestimates lightning density in some subtropical oceanic regions. F14 (Figure 2b) overestimates flash density over tropical oceans and underestimates flash density over a few Southern Hemisphere oceanic regions downstream from major continental areas by 50%–100%. Over land, F14 overestimates lightning density in the Amazon (by 50%–100%), central/sub-Saharan Africa (10%–100%), and parts of the Maritime Continent (10%–75%, barring the island of Borneo), but underestimates flash density in northern Africa as well as southern Asia by 50%–75%. F14 also underestimates lightning in coastal regions downstream of major continents in both hemispheres, poleward of approximately 30° latitude. Like F14, using S17 (Figure 2c) results in overestimates of flash density over tropical ocean (by 100% or more), yet underestimates flash density of 10%–75% are noted over subtropical ocean, mainly in the Southern Hemisphere. The S17 parameterization also underestimates lightning (by 10%–75%) over the Amazon, central Africa, and the Maritime Continent, where some of the most intense thunderstorms on Earth occur (Zipser et al., 2006). Underestimates of flash density using S17 become greater over land areas in the poleward directions (i.e., toward the subtropical latitudes). H_0 was accepted over approximately 9.5%, 15.5%, and 13.8% of the grid boxes in the study domain using for PR92, F14, and S17, respectively, and the fraction of grid boxes for which H_0 was accepted was greater over ocean compared to over land for all approaches evaluated herein (see the upper right portion of each panel in Figure 2).

The mean annual cycles for the northern and southern hemisphere were calculated using the domain-average flash density for each month separately in the two-year evaluation period (Figure 3**)**. The observed patterns show that more lightning occurs during the warm season in each hemisphere (JJA for the Northern Hemisphere and DJF for the Southern Hemisphere), which is in line with initial observations from the Global Lightning Mapper carried on the GOES-R satellite (Rudlosky et al., 2018) and earlier satellite lightning observation platforms (Cecil et al., 2014; Christian et al., 2003). In the Northern Hemisphere (Figure 3a), the peak observed flash density occurs for the month of June (7.36 fl. yr^{-1} km^{-2} $_{grid\_box}$) and the minimum flash density occurs for the month of January (1.39 fl. yr^{-1} km^{-2} $_{grid\_box}$). Each lightning parameterization exhibits a single peak throughout the annual cycle in the Northern Hemisphere; consistent with observations, the minimum flash density is found for the month of January for all parameterizations.

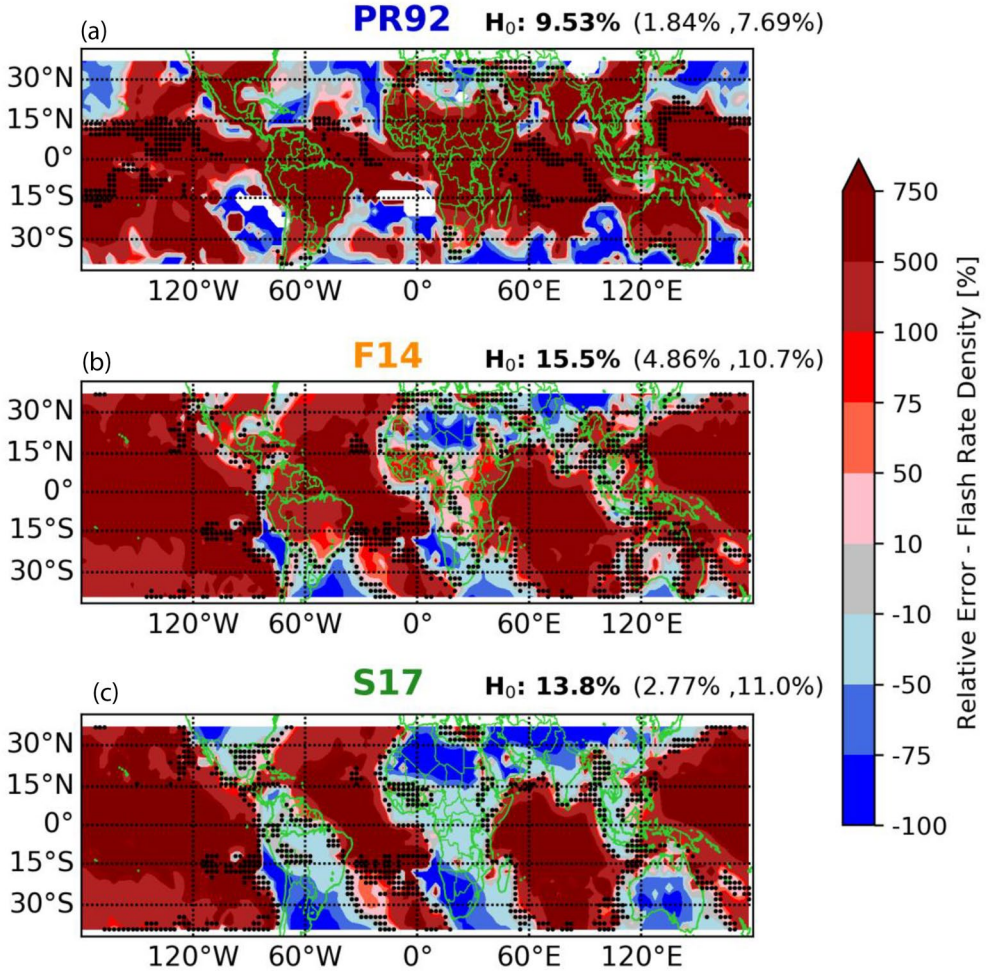

Figure 2. The average error in total lightning flash density (fl. yr^{-1} km^{-2} $_{grid\_box}$) for parameterizations by (a) PR92, (b) F14, and (c) S17 during the evaluation period (as in Figure 1). Blue shading (red shading) indicates areas where the parameterization underestimates (overestimates) observations. Black dots indicate grid boxes in which the null hypothesis (H_0) for equivalence of medians of the monthly samples of parameterized and observed lightning was not rejected at the 5% significance level (two-tailed probability). The fraction of grid boxes for which H_0 applies is shown in the upper right of each panel for the entire domain (bold) as well as for land and ocean areas, respectively, in parentheses.

However, the peak lightning indicated by each parameterization occurs in the month of August (lagging the observations-based peak by 2 months). The mean of the monthly flash density for the Northern Hemisphere (Figure 3a) is a factor of 12.1 greater than observations using PR92, 1.56 times greater using F14, and 0.93 times as large using S17. The temporal correlation with monthly observations is $r = 0.92$ for PR92, $r = 0.95$ for F14, and $r = 0.87$ for S17.

The observed annual cycle in the Southern Hemisphere (Figure 3b) features an absolute maximum in lightning in the month of December (5.83 fl. yr^{-1} $km^{-2}_{grid\_box}$) and an absolute minimum lightning in June (1.48 fl. yr^{-1} $km^{-2}_{grid\_box}$). The peak flash density is found in the month of December for PR92, whereas the peak is found in February for both F14 and S17. In contrast to observations, two local lightning maxima are found for the parameterizations in the Southern Hemisphere; the secondary peaks (by magnitude) occur in the month of February for PR92, in November for F14, and in December for S17. The absolute minimum flash density occurs in the month of July for PR92, in August for F14, and in July for S17. A small local minimum in lightning also occurs in January for PR92, in December for F14, and in January for S17. Compared to observations, the mean of the monthly flash density for the Southern Hemisphere (Figure 3b) is a factor

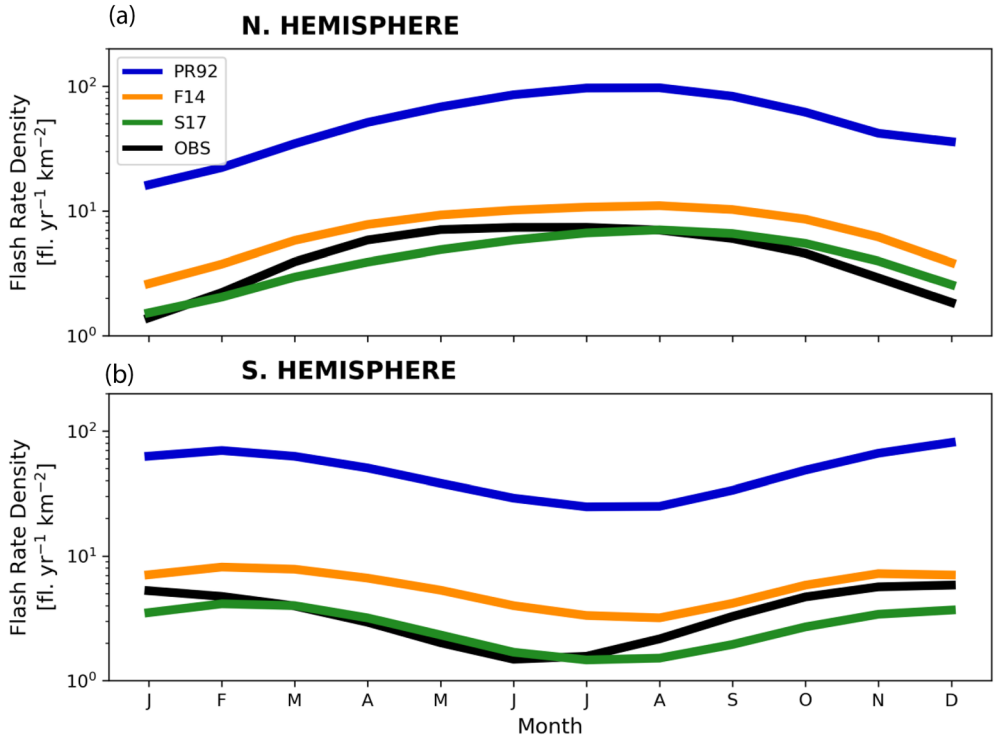

Figure 3. Observed (black, solid) and parameterized (colored, solid) mean annual cycles of domain-wide average total lightning flash density (fl. yr^{-1} km$^{-2}{}_{grid_box}$) (38°S–38°N, across all longitudes) for the evaluation period (as in Figure 1).

of 13.6 greater using PR92, 1.60 times greater using F14, and 0.77 times as great using S17. The temporal correlation with monthly observations is $r = 0.90$ for PR92, $r = 0.79$ for F14, and $r = 0.83$ for S17.

3.2. Total Lightning Density Spectra

The spectral distributions of flash density for observations and the three parameterizations are shown in Figure 4, where the binning has been carried out in logarithmic space (such that "visual integration" of the area under each curve corresponds to the frequency of occurrence). Moreover, land and ocean spectra have been computed separately from the full domain to highlight regional differences. The observed flash density spectrum for the full domain (Figure 4a) exhibits two local maxima (near 1 fl. yr^{-1} km$^{-2}{}_{grid_box}$ and 10 fl. yr^{-1} km$^{-2}{}_{grid_box}$, respectively). From examination of Figures 4b and 4c, the two peaks in the observed distribution for the full domain approximately correspond to separate "modes" over land and ocean that are separated by roughly an order of magnitude. The land-ocean contrast, defined as ratio of the median of the lightning distributions over land and ocean, is 22.9. Williams and Stanfill (2002) suggested that the land-ocean contrast in lightning climatology is a physical manifestation of differences in the Earth's surface, atmospheric thermodynamic background, and resultant differences in the dynamical and kinematic tendencies of deep convection that develops over land and oceans. Moreover, sensitivity of flash density to CCN concentrations has been shown for homogenous thermodynamic conditions over land and ocean (e.g., Stolz et al., 2017b, 2015; Thornton et al., 2017; Yuan et al., 2011), respectively, following an earlier "aerosol" hypothesis by Rosenfeld et al. (2008). The oceanic lightning spectrum (Figure 4b) depicts flash density values that overlap with land areas (e.g., in terms of magnitude). Finally, both the observed ocean and land lightning distributions also have long left-tail characteristics, which may be an artifact of spatial and temporal smoothing routines that were used in this study (e.g., following Cecil et al., 2014).

Parameterized domain-wide flash density spectra use separate relationships for land and ocean areas, and the parameterizations differ in terms of how they represent the distributions of total flash density over these regions. For PR92, the three-peak structure in lightning over ocean (with peaks near 0.03 fl. yr^{-1} km$^{-2}{}_{grid_box}$, 0.9 fl. yr^{-1} km$^{-2}{}_{grid_box}$, and >100 fl. yr^{-1} km$^{-2}{}_{grid_box}$) may indicate contributions from multiple components

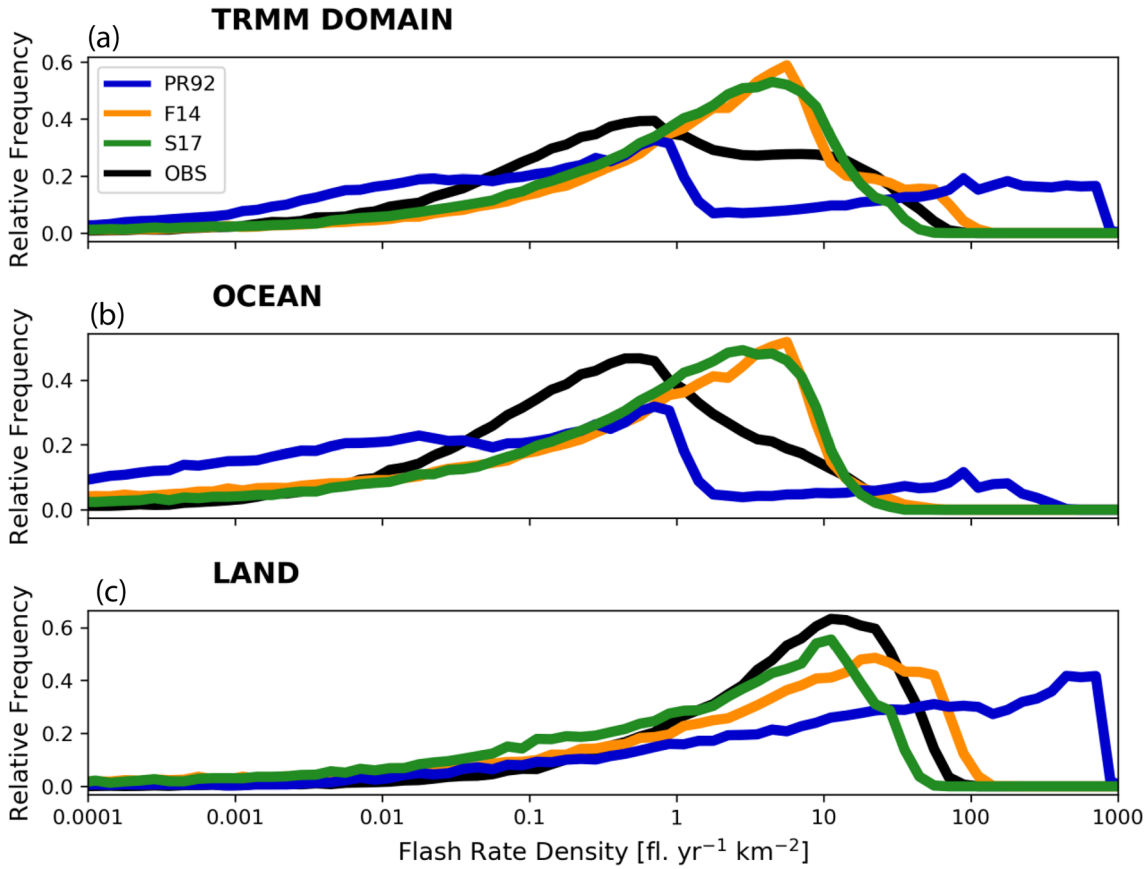

Figure 4. The probability density functions of total lightning flash density (fl. yr^{-1} km^{-2} $_{grid\_box}$) using logarithmic binning, accounting for all non-zero lightning values in grid boxes in (a) the full TRMM domain (38°S–38°N, across all longitudes), (b) over ocean, and (c) over land during the evaluation period (as in Figure 1). TRIM, tropical rain measuring mission.

of the tropical convective cloud top height distribution (e.g., Johnson et al., 1999). However, in the tropics/subtropics, lightning does not generally occur unless significant concentrations of ice/liquid hydrometeors exist above approximately 4–5 km altitude above mean sea level within the cloud. Therefore, the peak(s) for lower magnitudes in the PR92 oceanic lightning distribution may be spurious (to be discussed further in Section 4 below). For PR92 over land (Figure 4c), two peaks in lightning are apparent (near 90 fl. yr^{-1} km^{-2}$_{grid\_box}$ and approximately 700 fl. yr^{-1} km^{-2}$_{grid_box}$). The highest ocean mode (near 100 fl. yr^{-1} km^{-2}$_{grid\_box}$) in PR92 (seen in Figure 4b) is close to the peaks shown in the distribution over land. Similar overlap between ocean and land distributions is noted for F14 and S17, yet the ocean and land distributions separately for F14 and S17 can best be described as unimodal with considerable skewness. Over ocean (Figure 4b), the peaks in the lightning distributions shown for F14 and S17 occur between 1 and 10 fl. yr^{-1} km^{-2}$_{grid_box}$. Over land (Figure 4c), the peaks in the lightning distributions occur at approximately 30 fl. yr^{-1} km^{-2}$_{grid\_box}$ for F14 and 10 fl. yr^{-1} km^{-2}$_{grid_box}$ for S17. The land-ocean contrast is a factor of 596.0 for PR92, 6.02 for F14, and 2.81 for S17. Thus, PR92 greatly overestimates the observed land-ocean lightning contrast (given the spectral broadness of the underlying domain-wide lightning distribution), while F14 and S17 underestimate the land-ocean lightning contrast.

Inspection of Figure 4 reveals that errors in lightning estimates over oceanic regions (e.g., as shown in Figure 2) possibly result from the parameterizations overestimating the frequency of moderate to high lightning density (>1 fl. yr^{-1} km^{-2}$_{grid\_box}$) and underestimating the frequency of low to moderate lightning density (<1 fl. yr^{-1} km^{-2}$_{grid_box}$). For land areas shown in the spatial distributions (Figure 2), we noted that PR92 and F14 mostly overestimated flash density, on average, while S17 mostly underestimated flash density. In Figure 4c (over land), PR92 and F14 each overestimate the highest observed flash density (for values > 40–50 fl. yr^{-1} km^{-2}$_{grid_box}$) while S17 underestimates the highest values. All the parameterizations overestimate

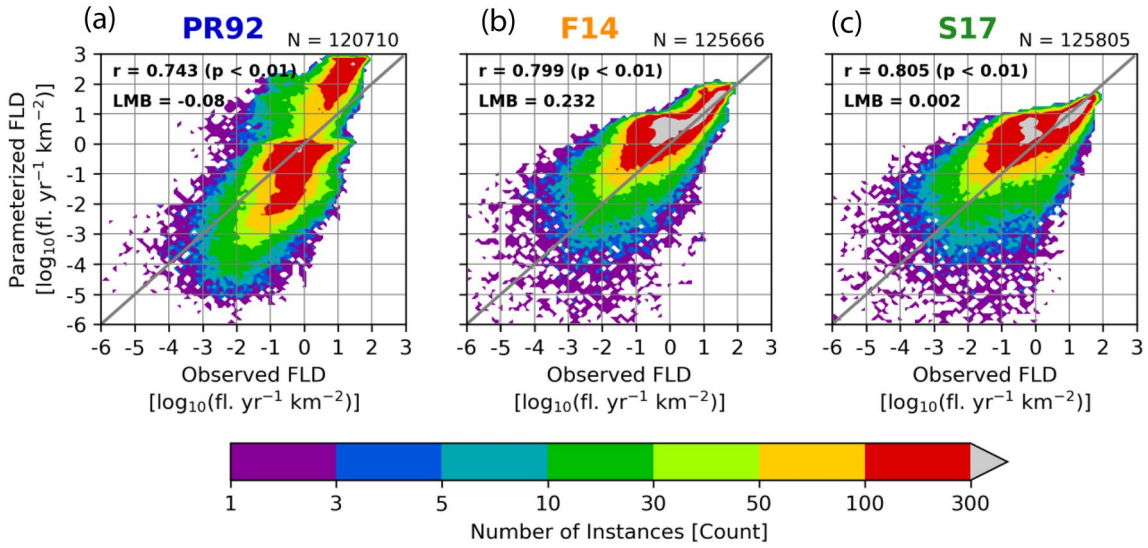

Figure 5. One-to-one, grid-point comparisons of observed total lightning flash density [fl. Yr^{-1} $km^{-2}{}_{grid\_box}$] vs. parameterized lightning flash density using (a) PR92, (b) F14, and (c) S17 during the evaluation period (as in Figure 1). The number of grid points sampled ("*N*") is in the upper right of each panel, while logarithmic mean bias ("LMB"), the linear Pearson correlation coefficient ("*r*"), and the probability value ("*p*") are provided in the upper left portion of each panel. Note the logarithmic scale on each horizontal and vertical axis for lightning flash density. The thin, solid gray diagonal line is the one-to-one line. Shaded contouring indicates the number of observations (also logarithmically scaled) and the color scale itself is uniform between each panel. LMB, logarithmic mean bias.

the frequency of flash density near 0.1 fl. yr^{-1} $km^{-2}{}_{grid\_box}$, with S17 showing the largest deviation in relative frequency for this magnitude over land.

3.3. One-to-One Comparison

By collating many pairs of flash density estimates (the parameterized value and observation) at each grid point for each of the 24 months of the evaluation period ($N > 100{,}000$), we assessed how well each parameterization handled spatial and temporal variance simultaneously. We find that parameterized and observed flash density are positively correlated on monthly timescales (Figure 5), with linear Pearson correlations of $r = 0.74$ for PR92, $r = 0.80$ for F14, and $r = 0.80$ for S17. Thus, the parameterizations account for 55%–64% of the observed spatiotemporal monthly flash density variance. The statistical significance of all aforementioned linear Pearson correlations surpassed a 5% significance level criterion, which is based on comparison with the hypothetical two-tailed probability that N random draws from an uncorrelated sampling distribution yields correlation exceeding the resulting r values; the relatively large data sample sizes analyzed here ($N > 100{,}000$) contribute to the robustness of these statistical findings (Wilks, 2011). The range of observed flash density spans more than five orders of magnitude. Two clusters are recognizable for PR92 (Figure 5a), whereas the distributions of F14 and S17 (Figures 5b and 5c) are more continuous when both components of spatial and temporal variability are considered together.

We quantify the relative error in flash density for each parameterization using logarithmic mean bias (LMB) as follows in Equation 6:

$$\mathrm{LMB} = 1 / N \cdot \sum_i \left(\log_{10}\left(y_i\right) - \log_{10}\left(x_i\right) \right) \tag{6}$$

where y_i and x_i are the ith parameterized and observed flash density values, respectively. We have chosen to represent the domain-wide bias in estimates using LMB since errors for low and high magnitudes are weighted equally. By this metric and averaging over the full domain, S17 has the smallest average error (+0.002) followed by PR92 (−0.08) and F14 (+0.232). Note that these domain-wide LMB results are indicative of parameterized lightning density estimates coming to within a factor of 2 (i.e., LMB~0.30) compared to observations for the tropical/subtropical domain between 38°S and 38°N. Yet from inspection of

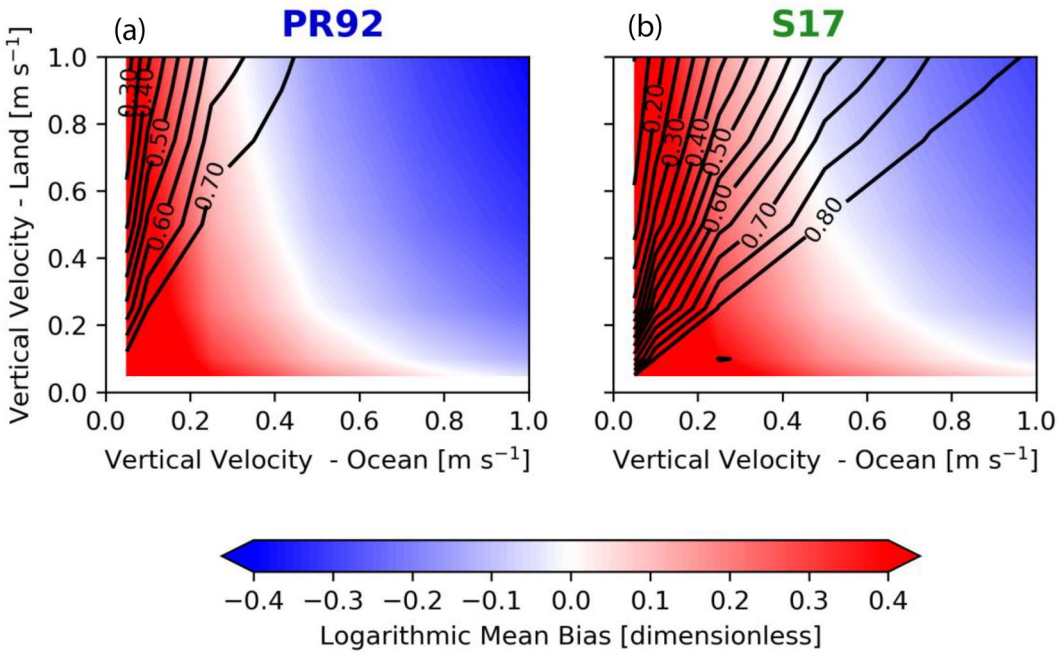

Figure 6. The distributions of the Logarithmic Mean Bias (shaded), and linear correlation coefficient (solid black with labels in-line; contour interval = 0.05) as a function of assumed vertical velocity (m s^{-1}) over land (*y*-axis) and ocean (*x*-axis).

Figures 4 and 5 together, errors over ocean and land areas compensate for one another in accounting for generally low values of LMB overall.

3.4. Sensitivity to the Choice of Vertical Velocity

Recall from Section 2.4 above, that PR92 and S17 require assumptions of "global" vertical velocity (i.e., w_{globe}) in order to derive estimates of thunderstorm area/number as well as convective area (i.e., following from Equation 1) over land and ocean. For the foregoing analysis, we used a constant value of +0.5 m s^{-1} over both land and ocean. To investigate the sensitivity of the flash density estimates produced by the PR92 and S17 parameterizations following the approach developed here, we re-computed the LMB and linear Pearson correlation for permutations of vertical velocity over land and ocean, respectively, with the results shown in Figure 6. The choice of vertical velocity in the range between +0.05 and 1 m s^{-1} over land and ocean, accounts for a range of outcomes from no average bias (i.e., LMB = 0) up to a difference between parameterized and observed flash density by a factor of approximately 2.5 (i.e., |LMB| = 0.4). For PR92, assuming w_{globe} = +0.5 m s^{-1} results in LMB of about −0.1 with correlation values of $r \sim 0.7$; using a lower vertical velocity assumption over ocean ($w \sim 0.4$ m s^{-1}) while keeping the value of 0.5 m s^{-1} over land (Figure 6a) results in reduction of LMB toward zero. For S17, the initial assumption of a constant updraft +0.5 m s^{-1} for both land and ocean falls very near to the curve of zero average error (i.e., white shading) that transects the parameter space, and meanwhile allows for a relatively high correlation for S17 (Figure 6b). The range of linear correlation values for all permutations of vertical velocities tested over land and ocean (+0.05–1.0 m s^{-1}) was r = 0.27–0.74 for PR92 and r = 0.10–0.85 for S17.

Williams and Stanfill (2002) presented results from aircraft penetrations of tropical oceanic and mid-latitude continental convective updrafts, respectively, and noted that maximum updrafts over land were systematically more intense by a factor of 2 compared to updrafts over ocean (at altitudes between cloud base and approximately 8 km altitude); one interpretation is that the average vertical motion in convective clouds over land is greater compared to over oceans. Following the trajectories of zero LMB in Figure 6 such that the ratio of vertical velocities over land and ocean is approximately equal to two (e.g., as dictated by Williams & Stanfill, 2002) results in a general decrease in the linear correlation coefficient, more so for S17.

Proceeding "down" the curve of zero LMB toward the lower right portion of each panel in Figure 6 results in maintaining relatively high linear correlation between parameterized and observed flash density, but assumptions of vertical velocity approaching 0 m s^{-1} for land and >1 m s^{-1} over ocean goes against the conventional understanding of deep tropical convective characteristics (e.g., Rutledge et al. 1992; Williams & Stanfill, 2002; Zipser & Lutz, 1994; Zipser et al., 2006). For the purpose of using the PR92 and S17 lightning parameterizations in this paper, assuming $w_{globe} = +0.5$ m s^{-1} (consistent with the median of vertical velocity observations collected during tropical convective cloud penetrations) seems appropriate.

4. Discussion

This study examined spatial, temporal, and spectral distributions of total lightning flash density calculated according to multiple different lightning parameterizations (Finney et al., 2014; Price & Rind, 1992; Stolz et al., 2017) as well as their performance in reproducing aspects of an observed monthly lightning climatology at 2.0 × 2.5° horizontal resolution, using a single reanalysis product, MERRA-2. The approach to estimate total flash density according to the aforementioned parameterizations is based on conversions from convective area/cloud area to more accurately reflect lightning in a grid box area in a single global atmospheric model. Without including dimensionless scaling coefficients, the results suggest that estimating lightning using model-based diagnostics indicative of the pre-convective environment (e.g., S17) generally matches or improves upon other approaches for lightning parameterization (i.e., by PR92 and F14) that incorporate cloud top height attributes or ice mass fluxes respectively. Murray et al. (2012) showed that artificial correction factors exceeding 2–4 orders of magnitude (cf., Table 2 of that study) were required to align model-predicted lightning estimates from PR92 with observations, when raw lightning flash rates calculated from cloud top height were normalized directly by grid box area (e.g., without accounting for convective fraction or the number of thunderstorm complexes within each model grid box). The results here also support that significant disparities between domain-wide averages of parameterized lightning and observations can be reduced by rigorously converting lightning estimates from storm-/cloud-scale parameterizations to appropriate grid box dimensions.

In past comparisons of lightning parameterizations in global models (e.g., Clark et al. 2017; Lopez, 2016; Meijer et al., 2001; Michalon et al., 1999; Murray et al., 2012; Tost et al., 2007), others have questioned whether the aforementioned differences between parameterized and observed lightning arise from the lightning parameterization, the convective parameterization, or some combination of the two (e.g., Tost et al., 2007). Each of the lightning parameterizations evaluated here predicted the timing of peak/minimum flash density 1–2 months after the observations in both the northern and southern hemispheres (Figure 3), which suggests that the model may be physically misrepresenting the timing of the most intense convection and quiescent periods in some areas. On the other hand, large differences in the mean flash density in each hemisphere (Figure 3), lightning spectra (Figure 4), as well as the land-ocean contrast in flash density (Figures 1 and 4) potentially highlights limitations of the various statistical parameterizations. It is difficult to confidently distinguish the source of residual errors found in this study because the MERRA-2 reanalysis meteorology (which is also subject to incomplete observations and model error) has been averaged/interpolated. Moreover, our results are derived from using a single global atmospheric model as an experimental control strategy. Future studies could seek to generalize the current approach by implementing a subset of global lightning parameterizations (e.g., while accounting for convective cloud fraction/area) in multiple global atmospheric models for comparison.

It is possible that there is sampling bias in lightning observations used by F14 and S17 (i.e., TRMM LIS) to derive the parameterizations evaluated here. We used a 2-year subset of LIS climatology to isolate lightning input that was not used in either of the original studies by F14 and S17, but F14 demonstrated that using a 5-year subset is more representative of the available total lightning climatology. Using LIS LRMTS as the observational benchmark for evaluation may favor F14 and S17 over PR92, possibly due the LIS instrument's sampling bias(es) being incorporated by F14 and S17 during training. A future evaluation could utilize the second LIS instrument flown onboard the international space station and/or the Global Lightning Mapper toward a more independent evaluation over a broader geographic domain, pending availability of chemical emissions inventories and a multi-year period of stable lightning observations by the aforementioned alternative lightning observation platforms. In addition, there are details surrounding aspects of our approach that could influence our results and are worth noting, and we discuss these aspects below.

Without model diagnostics to indicate the presence of lightning in a model grid box, assumptions for calculating lightning estimates in select modeled environments are required to account for when modeled convection produces lightning. For all parameterizations that we tested, we did not compute flash density in model grid boxes that did not meet both of the following criteria: the presence of conditional instability (NCAPE > 0.0 J kg^{-1} m^{-1}) and non-zero convective fraction (i.e., positive, non-zero moist-convective vertical mass flux). Note, strongly electrified convection is not likely to result within environments with small instability, favoring generally weak updrafts (Zipser, 1994). An additional assumption to mitigate occurrences of shallow or excessively deep WCD (WCD < 2,000 m or WCD > 5,000 m) was enforced for S17 alone because the S17 lightning parameterization was not trained using these marginal WCD values as in inputs. S17 documented that environments with WCD outside the identified range accounted for a relatively small fraction of total occurrences for lightning-producing convective features between the years 2004 and 2011 in the TRMM domain. In this study, outlier lightning estimates (generally larger than three standard deviations from the mean) were found using S17 when WCD in a grid box fell outside the WCD range of 2,000–5,000 m. As alluded to above, future studies using lightning observations that cover extratropical latitudes could eliminate the need to subset environments based on WCD.

We calculated the convective fraction from the grid-box average upward convective mass flux (convective fraction is not an explicit variable in the MERRA-2 reanalysis), and we acknowledge that our assumption of constant vertical velocity of +0.5 m s^{-1} throughout the study domain is crude (see Section 3.4). Vertical motions in deep convective clouds vary in space and time, even on monthly time scales. The results of a sensitivity test for constant vertical velocity over land and ocean here (Figure 6) support that domain-wide logarithmic mean bias statistics can be minimized when the assumed vertical velocity over land is approximately a factor of two greater than the assumed vertical velocity over ocean (e.g., Williams & Stanfill, 2002; Zipser & Lutz, 1994), yet the domain-wide linear correlation between parameterized and observed flash density decreased for these cases (from 0.70–0.80 to 0.50–0.60) using both PR92 and S17. We also noted that the low error bias statistics were paired with relatively high linear correlations when vertical velocity over land was reduced toward 0 m s^{-1} and the assumed vertical velocity over ocean was increased toward +1 m s^{-1}; however, this configuration of vertical velocity over land and ocean is physically unrealistic (e.g., based on historical observations).

From Equation 1, the convective fraction is inversely proportional to the chosen vertical velocity, such that increasing the vertical velocity reduces the convective fraction and vice versa. The findings of low domain-wide average error bias and high correlation for low vertical velocity over land and high vertical velocity over ocean can alternatively be interpreted as a need for greater convective fraction over land compared to over ocean. Previous studies (e.g., Boccippio et al., 2000; Liu et al., 2012; Williams et al., 2000) provide supporting observational evidence that thunderstorms are more widely separated in space over ocean compared to land. Thus, new methods to compute convective fraction/area should be explored for implementing global-scale lightning parameterizations that are based on convective area/thunderstorm area and spacing because the assumptions surrounding the convective area will impact domain-wide monthly lightning distributions (e.g., the land-ocean contrast).

The parameterizations that were analyzed in this study represented the land-ocean lightning contrast with varying levels of precision, especially at the low-end tail of the distribution (Figures 4 and 5). It is possible that the observation strategy of TRMM paired with spatial and temporal smoothing methodology (e.g., Cecil et al., 2014) may contribute to some of the apparent disagreement between the observations and lightning parameterizations. Given that the TRMM LIS's minimum detectable flash rate is approximately 0.7 fl. min^{-1} within a 0.5° latitude-longitude grid box (e.g., Cecil et al., 2014), a portion of the lightning spectrum is "missed" in observations (which truncates the range of observable low-magnitude lightning events). It remains to be shown whether these low lightning counts or null events in observations correspond to events with negligible instability and/or minimal convective fraction over any given area. Accounting for these issues in grid-based analyses and modeling should improve multi-mode spectral lightning representations altogether (e.g., as part of future approaches to implement lightning parameterizations in global models).

Improvements are necessary to reduce errors in lightning estimates over both continents and oceans and to subsequently enable more accurate predictions of the evolution of atmospheric chemistry using global atmospheric models. There is also considerable interest in understanding how lightning will respond to

future climate change (Finney et al., 2018; Price, 2013; Romps et al., 2014; Williams, 2005, 2012; Williams et al., 2019). Recent literature illustrates that future lightning projections show appreciable increases or decreases of lightning frequency depending on the lightning parameterization chosen (Clark et al., 2017; Romps, 2019), resulting from the parameterizations' different underlying sensitivities (e.g., to environmental factors and/or cloud properties, etc.). Most major climate models currently either provide options for including online aerosol microphysics or the models provide estimates of non-size resolved aerosol tracers, at minimum; therefore, it is possible to estimate CCN concentrations using assumed size distributions for each aerosol species to support implementation of global lightning parameterizations that utilize CCN concentrations as input.

For the current study, we used modeled vertical moist convective mass flux to diagnose the cloud top height and the resulting flash density estimates using PR92 showed appreciable errors in the land-ocean lightning contrast (more than a factor of 25 greater than observed) as well as in the spectral representation of lightning (Figures 1;3; and 4). One-to-one comparison between PR92 and observations (e.g., Figure 5) indicated the weakest linear Pearson correlation and a moderate average error bias (despite the largest error variance overall). In this study, there were indications that the PR92 parameterization produces a greater relative frequency of low lightning rates (e.g., Figure 4), compared to either F14 or S17, based on the presence of positive moist convective vertical mass flux. However, lightning is not likely to develop within modest cumuli in the tropics/subtropics due to the apparently lack of robust mixed-phase microphysical development (e.g., Liu et al., 2012, 2010; Rutledge et al., 1992; Stolz et al., 2015) to promote charge separation. Here is a potential shortcoming of parameterizing lightning in the tropics using the PR92 approach without a minimum cloud top height threshold. A more recent approach to estimate flash density based on vertical ice mass flux by F14 depicted generally good agreement with observed spectral and temporal lightning patterns and the closest approximation of the observed land-ocean lightning contrast; one-to-one comparison between F14 and observations indicated greater linear correlation than PR92, but the average error bias was the largest out of the three parameterizations tested here. Parameterizing flash density using environmental factors and CCN according to S17 resulted in the highest linear correlation, the lowest average error bias, yet an underestimation of the land-ocean lightning contrast, possibly a result of S17's decision to train the statistical relationships based on flash density without accounting for coastal regions separately. For future work, we recommend isolating and quantifying lightning in coastal regions for a third regional parameterization component (i.e., developing land, coastal, and oceanic lightning relationships instead of developing only two relationships for land and ocean), given that the coastal regions consistently exhibit environmental characteristics that are intermediate between land and remote oceanic conditions (e.g., Stolz et al., 2015).

Based on the findings of this study, flash density estimates from PR92 were generally less consistent with observations, whereas S17 and F14 were more representative of the land-ocean contrast and in terms of agreement with observed spatiotemporal lightning patterns. More accurate representations of lightning-climate coupling as well as characterizations of lightning's interaction with atmospheric chemistry in future global atmospheric modeling systems may be possible using environmental factors (CAPE, shear and warm cloud depth), CCN concentrations, vertical cloud ice flux, or some combination of these inputs (while accounting for thunderstorm area), as opposed to using cloud top height alone.

Data Availability Statements

GEOS-Chem v12.0.3 source code that was used for this study can be retrieved from http://doi.org/10.5281/zenodo.1464210. Three-hourly, three-dimensional MERRA-2 reanalysis data on model levels are available from NASA's Global Modeling and Assimilation Office (GMAO), https://gmao.gsfc.nasa.gov/. The LIS/OTD gridded lightning climatology (Low-Resolution Monthly Time Series) was downloaded at nominal 2.5 × 2.5° horizontal resolution and re-gridded for the purpose of this study; the native data are available from the NASA Global Hydrology Resource Center (GHRC), http://dx.doi.org/10.5067/LIS/LIS-OTD/DATA309.

Acknowledgments
The authors are grateful for the commitments of two anonymous reviewers who supplied valuable feedback toward improving this manuscript. Funding for this work was provided by NASA grant NNX17AH62G.

References

Adams, P. J., & Seinfeld, J. H. (2002). Predicting global aerosol size distributions in general circulation models. *Journal of Geophysical Research*, *107*(D19), 4370. https://doi.org/10.1029/2001JD001010

Albrecht, R. I., Goodman, S. J., Buechler, D. E., Blakeslee, R. J., & Christian, H. J. (2016). Where are the lightning hotspots on Earth? *Bulletin of the American Meteorological Society*, *97*(11), 2051–2068. https://doi.org/10.1175/BAMS-D-14-00193.1

Allen, D. J., & Pickering, K. E. (2002). Evaluation of lightning flash rate parameterizations for use in a global chemical transport model. *Journal of Geophysical Research*, *107*(D23), 4711. https://doi.org/10.1029/2002JD002066

Barthe, C., Deierling, W., & Barth, M. C. (2010). Estimation of total lightning from various storm parameters: A cloud-resolving model study. *Journal of Geophysical Research*, *115*(D24), D24202. https://doi.org/10.1029/2010JD014405

Boccippio, D. J., Goodman, S. J., & Heckman, S. (2000). Regional differences in tropical lightning distributions. *Journal of Applied Meteorology*, *39*(12), 2231–2248. https://doi.org/10.1175/1520-0450(2001)040<2231:RDITLD>2.0.CO;2

Boccippio, D. J., Koshak, W. J., & Blakeslee, R. J. (2002). Performance assessment of the optical transient detector and lightning imaging sensor. Part I: Predicted diurnal variability. *Journal of Atmospheric and Oceanic Technology*, *19*(9), 1318–1332. https://doi.org/10.1175/1520-0426(2002)019<1318:PAOTOT>2.0.CO;2

Bosilovich, M. G., Akella, S., Coy, L., Cullather, R., Draper, C., Gelaro, R., et al. (2015). MERRA-2: Initial evaluation of the climate. Technical report Series on global modeling and data assimilation (Vol. 43, pp.153). Retrieved from https://ntrs.nasa.gov/citations/20160005045

Cecil, D. J. (2006). *LIS/OTD 2.5 degree low resolution monthly climatology time Series (LRMTS)*. Huntsville, AL: NASA Global Hydrology Resource Center DAAC. http://dx.doi.org/10.5067/LIS/LIS-OTD/DATA309

Cecil, D. J., Buechler, D. E., & Blakeslee, R. J. (2014). Gridded lightning climatology from TRMM- LIS and OTD: Dataset description. *Atmospheric Research*, *135–136*, 404–414. https://doi.org/10.1016/j.atmosres.2012.06.028

Christian, H., Blakeslee, R. J., & Goodman, S. J. (1992). *Lightning imaging sensor for the Earth observing system* (p. 44). NASA TM-4350. Retrieved from https://ntrs.nasa.gov/api/citations/19920010794/downloads/19920010794.pdf

Christian, H. J., Boccippio, D. J., Boeck, W. L., Buechler, D. E., Driscoll, K. L., et al. (2003). Global frequency and distribution of lightning as observed from space by the optical transient detector. *Journal of Geophysical Research*, *108*(D1), 4005. https://doi.org/10.1029/2002JD002347

Clark, S. K., Ward, D. S., & Mahowald, N. M. (2017). Parameterization-based uncertainty in future lightning flash density. *Geophysical Research Letters*, *44*(6), 2893–2901. https://doi.org/10.1002/2017GL073017

Crippa, M., Janssens-Maenhout, G., Dentener, F., Guizzardi, D., Sindelarova, K., Muntean, M., et al. (2016). Forty years of improvements in European air quality: Regional policy-industry interactions with global impacts. *Atmospheric Chemistry and Physics*, *16*(6), 3825–3841. https://doi.org/10.5194/acp-16-3825-2016

D'Andrea, S. D., Häkkinen, S. A. K., Westervelt, D. M., Kuang, C., Levin, E. J. T., Kanawade, V. P., et al. (2013). Understanding global secondary organic aerosol amount and size-resolved condensational behavior. *Atmospheric Chemistry and Physics*, *13*(22), 11519–11534. https://doi.org/10.5194/acp-13-11519-2013

Finney, D. L., Doherty, R. M., Wild, O., & Abraham, N. L. (2016). The impact of lightning on tropospheric ozone chemistry using a new global lightning parameterization. *Atmospheric Chemistry and Physics*, *16*(12), 7507–7522. https://doi.org/10.5194/acp-16-7507-2016

Finney, D. L., Doherty, R. M., Wild, O., Huntrieser, H., Pumphrey, H. C., & Blyth, A. M. (2014). Using cloud ice flux to parametrise large-scale lightning. *Atmospheric Chemistry and Physics*, *14*, 12665–12682. https://doi.org/10.5194/acp-14-12665-2014

Finney, D. L., Doherty, R. M., Wild, O., Stevenson, D. S., MacKenzie, I. A., & Blyth, A. M. (2018). A projected decrease in lightning under climate change. *Nature Climate Change*, *8*(3), 210–213. https://doi.org/10.1038/s41558-018-0072-6

Gelaro, R., McCarty, W., Suárez, M. J., Todling, R., Molod, A., Takacs, L., et al. (2017). The modern-era retrospective analysis for research and applications, version 2 (MERRA-2). *Journal of Climate*, *30*(14), 5419–5454. https://doi.org/10.1175/JCLI-D-16-0758.1

Grewe, V., Brunner, D., Dameris, M., Grenfell, J. L., Hein, R., Shindell, D., & Staehelin, J. (2001). Origin and variability of upper tropospheric nitrogen oxides and ozone at northern mid-latitudes. *Atmospheric Environment*, *35*(20), 3421–3433. https://doi.org/10.1016/S1352-2310(01)00134-0

Guenther, A. B., Jiang, X., Heald, C. L., Sakulyanontvittaya, T., Duhl, T., Emmons, L. K., & Wang, X. (2012). The model of emissions of gases and aerosols from nature version 2.1 (MEGAN2.1): An extended and updated framework for modeling biogenic emissions. *Geoscientific Model Development*, *5*(2), 1471–1492. https://doi.org/10.5194/gmdd-5-1503-2012

Jaeglé, L., Quinn, P. K., Bates, T. S., Alexander, B., & Lin, J.-T. (2011). Global distribution of sea salt aerosols: New constraints from in situ and remote sensing observations. *Atmospheric Chemistry and Physics*, *11*(7), 3137–3157. https://doi.org/10.5194/acp-11-3137-2011

Johnson, R. H., Rickenbach, T. M., Rutledge, S. A., Ciesielski, P. E., & Schubert, W. H. (1999). Trimodal characteristics of tropical convection. *Journal of Climate*, *12*(8), 2397–2418. https://doi.org/10.1175/1520-0442(1999)012<2397:TCOTC>2.0.CO;2

Kodros, J. K., & Pierce, J. R. (2017). Important global and regional differences in aerosol cloud-albedo effect estimates between simulations with and without prognostic aerosol microphysics: Differences in cloud-Albedo aerosol indirect effect. *Journal of Geophysical Research: Atmospheres*, *122*(7), 4003–4018. https://doi.org/10.1002/2016JD025886

Kuhns, H., Knipping, E. M., & Vukovich, J. M. (2005). Development of a United States–Mexico emissions inventory for the big bend regional aerosol and visibility observational (BRAVO) study. *Journal of the Air and Waste Management Association*, *55*(5), 677–692. https://doi.org/10.1080/10473289.2005.10464648

Kummerow, C., Barnes, W., Kozu, T., Shiue, J., & Simpson, J. (1998). The tropical rainfall measuring mission (TRMM) sensor package. *Journal of Atmospheric and Oceanic Technology*, *15*(3), 809–817. https://doi.org/10.1175/1520-0426(1998)015<0809:TTRMMT>2.0.CO;2

Latham, J., Petersen, W. A., Deierling, W., & Christian, H. J. (2007). Field identification of a unique globally dominant mechanism of thunderstorm electrification. *Quarterly Journal of the Royal Meteorological Society*, *133*(627), 1453–1457. https://doi.org/10.1002/qj.133

LeMone, M. A., & Zipser, E. J. (1980). Cumulonimbus vertical velocity events in GATE. Part I: Diameter, intensity and mass flux. *Journal of the Atmospheric Sciences*, *37*(11), 2444–2457. https://doi.org/10.1175/1520-0469(1980)037<2444:CVVEIG>2.0.CO.2

Liu, C., Cecil, D. J., Zipser, E. J., Kronfeld, K., & Robertson, R. (2012). Relationships between lightning flash rates and radar reflectivity vertical structures in thunderstorms over the tropics and subtropics. *Journal of Geophysical Research*, *117*(D6), D06212. https://doi.org/10.1029/2011JD017123

Liu, C., Williams, E. R., Zipser, E. J., & Burns, G. (2010). Diurnal variations of global thunderstorms and electrified shower clouds and their contribution to the global electrical circuit. *Journal of the Atmospheric Sciences*, *67*(2), 309–323. https://doi.org/10.1175/2009JAS3248.1

Liu, C., Zipser, E. J., Cecil, D. J., Nesbitt, S. W., & Sherwood, S. (2008). A cloud and precipitation feature database from 9 years of TRMM observations. *Journal of Applied Meteorology and Climatology*, *47*(10), 2712–2728. https://doi.org/10.1175/2008JAMC1890.1

Li, M., Zhang, Q., Kurokawa, J., Woo, J.-H., He, K., Lu, Z., et al. (2017). MIX: a mosaic Asian anthropogenic emission inventory under the international collaboration framework of the MICS-Asia and HTAP. *Atmospheric Chemistry and Physics*, *17*(2), 935–963. https://doi.org/10.5194/acp-17-935-2017

Lopez, P. (2016). A lightning parameterization for the ECMWF integrated forecasting system. *Monthly Weather Review*, *144*(9), 3057–3075. https://doi.org/10.1175/MWR-D-16-0026.1

MacGorman, D. R., & Rust, W. D. (1998). *The electrical nature of storms* (p. 432). Oxford University Press.
Marais, E. A., & Wiedinmyer, C. (2016). Air quality impact of diffuse and inefficient combustion emissions in Africa (DICE-Africa). *Environmental Science and Technology*, *50*(19), 10739–10745. https://doi.org/10.1021/acs.est.6b02602
McCaul, E. W., Goodman, S. J., LaCasse, K. M., & Cecil, D. J. (2009). Forecasting lightning threat using cloud-resolving model simulations. *Weather and Forecasting*, *24*(3), 709–729. https://doi.org/10.1175/2008WAF2222152.1
Meijer, E. W., van Velthoven, P. F. J., Brunner, D. W., Huntrieser, H., & Kelder, H. (2001). Improvement and evaluation of the parameterisation of nitrogen oxide production by lightning. *Physics and Chemistry of the Earth*, *26*(8), 577–583. https://doi.org/10.1016/S1464-1917(01)00050-2
Michalon, N., Nassif, A., Saouri, T., Royer, J. F., & Pontikis, C. A. (1999). Contribution to the climatological study of lightning. *Geophysical Research Letters*, *26*(20), 3097–3100. https://doi.org/10.1029/1999GL010837
Murray, L. T., Jacob, D. J., Logan, J. A., Hudman, R. C., & Koshak, W. J. (2012). Optimized regional and interannual variability of lightning in a global chemical transport model constrained by LIS/OTD satellite data. *Journal of Geophysical Research*, *117*(D20), D20307. https://doi.org/10.1029/2012JD017934
Pai, S. J., Heald, C. L., Pierce, J. R., Farina, S. C., Marais, E. A., Jimenez, J. L., et al. (2020). An evaluation of global organic aerosol schemes using airborne observations. *Atmospheric Chemistry and Physics Discussions*, *20*, 2637–2665. https://doi.org/10.5194/acp-20-2637-2020
Petersen, W. A., Christian, H. J., & Rutledge, S. A. (2005). TRMM observations of the global relationship between ice water content and lightning. *Geophysical Research Letters*, *32*(14), L14819. https://doi.org/10.1029/2005GL023236
Petersen, W. A., & Rutledge, S. A. (2001). Regional variability in tropical convection: Observations from TRMM. *Journal of Climate*, *14*(17), 3566–3586. https://doi.org/10.1175/1520-0442(2001)014<3566:RVITCO>2.0.CO.2
Pierce, J. R., & Adams, P. J. (2009). Uncertainty in global CCN concentrations from uncertain aerosol nucleation and primary emission rates. *Atmospheric Chemistry and Physics*, *9*(4), 1339–1356. https://doi.org/10.5194/acp-9-1339-2009
Pierce, J. R., Evans, M. J., Scott, C. E., D'Andrea, S. D., Farmer, D. K., Sweitlicki, E., & Spracklin, D. V. (2013). Weak global sensitivity of cloud condensation nuclei and the aerosol indirect effect to Criegee + SO2 chemistry. *Atmospheric Chemistry and Physics*, *13*(6), 3163–3176. https://doi.org/10.5194/acp-13-3163-2013
Price, C. G. (2013). Lightning applications in weather and climate research. *Surveys in Geophysics*, *34*(6), 755. https://doi.org/10.1007/s10712-012-9218-7
Price, C., Penner, J., & Prather, M. (1997). NOx from lightning: 1. Global distribution based on lightning physics. *Journal of Geophysical Research*, *102*(D5), 5929–5941. https://doi.org/10.1029/96JD03504
Price, C., & Rind, D. (1992). A simple lightning parameterization for calculating global lightning distributions. *Journal of Geophysical Research*, *97*(D9), 9919–9933. https://doi.org/10.1029/92JD00719
Price, C., & Rind, D. (1993). What determines the cloud-to-ground fraction in thunderstorms? *Geophysical Research Letters*, *20*(6), 463–466. https://doi.org/10.1029/93GL00226
Price, C., & Rind, D. (1994). Modeling global lightning distributions in a general circulation model. *Monthly Weather Review*, *122*(8), 1930–1939. https://doi.org/10.1175/1520-0493(1994)122<1930:MGLDIA>2.0.CO;2
Randerson, J. T., van der Werf, G. R., Giglio, L., Collatz, G. J., & Kasibhatla, P. S. (2017). *Global fire emissions Database, version 4.1 (GFEDv4)*. Oak Ridge, TN: ORNL DAAC. https://doi.org/10.3334/ORNLDAAC/1293
Romps, D. M. (2019). Evaluating the future of lightning in cloud-resolving models. *Geophysical Research Letters*, *46*(24), 14863–14871. https://doi.org/10.1029/2019GL085748
Romps, D. M., Seeley, J. T., Vollaro, D., & Molinari, J. (2014). Projected increase in lightning strikes in the United States due to global warming. *Science*, *346*(6211), 851–854. https://doi.org/10.1126/science.1259100
Rosenfeld, D., Lohmann, U., Raga, G. B., O'Dowd, C. D., Kulmala, M., Fuzzi, S., et al. (2008). Flood or drought: How do aerosols affect precipitation? *Science*, *321*(5894), 1309–1313. https://doi.org/10.1126/science.1160606
Rudlosky, S. D., Goodman, S. J., Virts, K. S., & Bruning, E. C. (2018). Initial geostationary lightning mapper observations. *Geophysical Research Letters*, *46*(2), 1097–1104. https://doi.org/10.1029/2018GL081052
Rutledge, S. A., Williams, E. R., & Keenan, T. D. (1992). The down under Doppler and electricity experiment (DUNDEE): Overview and preliminary results. *Bulletin of the American Meteorological Society*, *73*(1), 3–16. https://doi.org/10.1175/1520-0477(1992)073<0003:TDUDAE>2.0.CO;2
Schumann, U., & Huntrieser, H. (2007). The global lightning-induced nitrogen oxides source. *Atmospheric Chemistry and Physics*, *7*, 3823–3907. http://www.atmos-chem-phys.net/7/3823/2007/
Stolz, D. C., Rutledge, S. A., & Pierce, J. R. (2015). Simultaneous influences of thermodynamics and aerosols on deep convection and lightning in the tropics. *Journal of Geophysical Research: Atmospheres*, *120*(12), 6207–6231. https://doi.org/10.1002/2014JD023033
Stolz, D. C., Rutledge, S. A., Pierce, J. R., & van den Heever, S. C. (2017). A global lightning parameterization based on statistical relationships among environmental factors, aerosols, and convective clouds in the TRMM climatology. *Journal of Geophysical Research: Atmospheres*, *122*(14), 7461–7492. https://doi.org/10.1002/2016JD026220
Stolz, D. C., Rutledge, S. A., Xu, W., & Pierce, J. R. (2017). Interactions between the MJO, aerosols, and convection over the central Indian Ocean. *Journal of the Atmospheric Sciences*, *74*(2), 353–374. https://doi.org/10.1175/JAS-D-16-0054.1
Takahashi, T. (1978). Riming electrification as a charge generation mechanism in thunderstorms. *Journal of the Atmospheric Sciences*, *35*(8), 1536–1548. https://doi.org/10.1175/1520-0469(1978)035<1536:REAACG>2.0.CO;2
Thornton, J. A., Virts, K. S., Holzworth, R. H., & Mitchell, T. P. (2017). Lightning enhancement over major oceanic shipping lanes. *Geophysical Research Letters*, *44*(17), 9102–9111. https://doi.org/10.1002/2017GL074982
Tost, H., Jöckel, P., & Lelieveld, J. (2007). Lightning and convection parameterisations – Uncertainties in global modelling. *Atmospheric Chemistry and Physics*, *7*(3), 4553–4568. https://doi.org/10.5194/acp-7-4553-2007
Trivitayanurak, W., Adams, P. J., Spracklen, D. V., & Carslaw, K. S. (2008). Tropospheric aerosol microphysics simulation with assimilated meteorology: Model description and intermodel comparison. *Atmospheric Chemistry and Physics*, *8*(12), 3149–3168. https://doi.org/10.5194/acp-8-3149-2008
Wilks, D. S. (2011). *Statistical methods in the atmospheric sciences* (3rd ed., p. 675). Oxford: Academic Press
Williams, E. R. (1985). Large-scale charge separation in thunderclouds. *Journal of Geophysical Research*, *90*(D4), 6013–6025. https://doi.org/10.1029/JD090iD04p06013
Williams, E. R. (2005). Lightning and Climate: A review. *Atmospheric Research*, *76*(1–4), 272–287. https://doi.org/10.1016/j.atmosres.2004.11.014
Williams, E. R. (2012). *Franklin lecture: Lightning and climate* (p. 70). San Francisco, CA: AGU Fall Meeting. Retrieved from http://fallmeeting.agu.org/2012/events/franklinlecture-ae31a-lightning-and-climate-video-on-demand/

Williams, E. R., Guha, A., Boldi, R., Christian, H., & Buechler, D. (2019). Global lightning activity and the hiatus in global warming. *Journal of Atmospheric and Solar-Terrestrial Physics*, *189*, 27–34. https://doi.org/10.1016/j.jastp.2019.03.011

Williams, E. R., Rothkin, K., Stevenson, D., & Boccippio, D. (2000). Global lightning variations caused by changes in thunderstorm flash rate and by changes in the number of thunderstorms. *Journal of Applied Meteorology*, *39*(12), 2223–2230. https://doi.org/10.1175/1520-0450(2001)040<2223:GLVCBC>2.0.CO.2

Williams, E. R., & Stanfill, S. (2002). The physical origin of the land-ocean contrast in lightning activity. *Comptes Rendus Physique*, *3*(10), 1277–1292. https://doi.org/10.1016/S1631-0705(02)01407-X

Yuan, T., Remer, L. A., Pickering, K. E., & Yu, H. (2011). Observational evidence of aerosol enhancement of lightning activity and convective invigoration. *Geophysical Research Letters*, *38*(4), L04701. https://doi.org/10.1029/2010GL046052

Zender, C. S., Miller, R. L. L., & Tegen, I. (2004). Quantifying mineral dust mass budgets: Terminology, constraints, and current estimates. *Eos*, *85*(48), 509–512. https://doi.org/10.1029/2004EO480002

Zipser, E. J. (1994). Deep cumulonimbus cloud systems in the tropics with and without lightning. *Monthly Weather Review*, *122*(8), 1837–1851. https://doi.org/10.1175/1520-0493(1994)122<1837:DCCSIT>2.0.CO.2

Zipser, E. J., Cecil, D. J., Liu, C., Nesbitt, S. W., & Yorty, D. P. (2006). Where are the most intense thunderstorms on Earth? *Bulletin of the American Meteorological Society*, *87*(8), 1057–1072. https://doi.org/10.1175/BAMS-87-8-1057

Zipser, E. J., & Lutz, K. R. (1994). The vertical profile of radar reflectivity of convective cells: A strong indicator of storm intensity and lightning probability? *Monthly Weather Review*, *122*(8), 1751–1759. https://doi.org/10.1175/1520-0493(1994)122<1751:TVPORR>2.0.CO;2